Autocrine fibronectin directs matrix assembly and crosstalk between cell–matrix and cell–cell adhesion in vascular endothelial cells

Botond Cseh, Samantha Fernandez-Sauze*, Dominique Grall, Sébastien Schaub, Eszter Doma and Ellen Van Obberghen-Schilling‡

University of Nice-Sophia Antipolis, CNRS UMR 6543, Centre Antoine Lacassagne, 33 Avenue de Valombrose, 06189 Nice, France
*Present address: Inserm UMR911, Faculté de Médecine, 27 Bd J. Moulin 13385 Marseille, France
‡Author for correspondence (ellen.van-obberghen@unice.fr)

Accepted 9 August 2010
Journal of Cell Science 123, 3989-3999

doi:10.1242/jcs.073346

Summary

Cellular fibronectin (cFN) variants harboring extra FN type 3 repeats, namely extra domains B and A, are major constituents of the extracellular matrix around newly forming blood vessels during development and angiogenesis. Their expression is induced by angiogenic stimuli and their assembly into fibrillar arrays is driven by cell-generated tension at α5β1 integrin-based adhesions. Here, we examined the role and functional redundancy of cFN variants in cultured endothelial cells by isoform-selective RNA interference. We show that FN fibrillogenesis is a cell-autonomous process whereby basally directed secretion and assembly of cellular FN are tightly coupled events that play an important role not only in signaling at cell–matrix adhesions but also at cell–cell contacts. Silencing of cFN variants differentially affects integrin usage, cell spreading, motility and capillary morphogenesis in vitro. cFN-deficient cells undergo a switch from α5β1- to αvβ3-based adhesion, accompanied by a Src-regulated disruption of adherens junctions. These studies identify a crucial role for autocrine FN in subendothelial matrix assembly and junctional integrity that provides spatially and temporally restricted control of endothelial plasticity during angiogenic blood vessel remodeling.

Key words: Adhesion, Fibrillogenesis, Fibronectin, Vascular endothelial cell

Introduction

Endothelial cells are exquisitely sensitive to their extracellular matrix (ECM) environment for growth, survival and organization into functional vascular networks during development and angiogenic blood vessel remodeling. The ECM provides not only an adhesive substrate for integrins and transmembrane proteoglycans but also a platform for transduction of intracellular signaling events that regulate a host of cellular functions. Although certain ECM components (e.g. laminin) appeared early in evolution, fibronectin (FN), a dimeric glycoprotein of 440–560 kDa, emerged only in vertebrates with an endothelial-cell-lined circulatory system (Whittaker et al., 2006). Genetic studies in mice and fish have pointed to a fundamental role for FN and its primary receptor, the α5β1 integrin, in early blood vessel development and vascular physio/pathology (for reviews, see Astrof and Hynes, 2009; Hynes, 2007). FN-null mice die at embryonic day 9.5 with severe cardiovascular defects (George et al., 1993) and α5-null mice display the most severe vascular defects of all the α-encoding integrin genes.

FN exists in two forms, plasma FN, a soluble form produced solely by hepatocytes that circulates at high concentrations, and cellular FN (cFN) produced by a subset of cells during development in zones of active morphogenesis and tissue remodeling (Ffrench-Constant and Hynes, 1989; Glukhova et al., 1989). Following embryonic development, the production of cFN largely shuts down, only to be turned on in a spatially and temporally restricted manner under certain physiological or pathological conditions, such as angiogenesis (Peters et al., 1996; Peters and Hynes, 1996). A major difference between cFN and plasma FN is the presence in cFN of alternatively spliced exons, including EDB and EDA (extra domains B and A, also termed EIIIB/EDII and EIIIA/EDI), each encoding a single FN type III repeat (see Pankov and Yamada, 2002). FN proteins containing the extra domain regions are among the most specific markers of angiogenic blood vessels to date and well suited for tumor-targeting strategies (Neri and Bicknell, 2005; Villa et al., 2008). Although the extra domains are highly conserved among vertebrates, their functions remain largely enigmatic (White et al., 2008; Wierzbicka-Patynowski and Schwarzbauer, 2003). Individually, EDB- and EDA-null mice are viable, fertile and have no apparent defects in physiological or tumor angiogenesis (Astrof et al., 2004; Fukuda et al., 2002; Muro et al., 2003; Tan et al., 2004). However, mice lacking both EDA and EDB (which continue to express FN-lacking EDB and EDA domains) die at embryonic day 10.5 owing to defects in embryonic and yolk sac vessels, heart defects and failure of vessels to invade the brain parenchyma (Astrof et al., 2007), indicating that the presence or absence of EDB and EDA exons alters the function of FN.

FN functions as a multidimensional fibrillar matrix, and the architecture of the network itself contributes to the control of cell behavior. Ongoing polymerization is essential for the deposition of other matrix proteins, including fibrinogen (Pereira et al., 2002), collagens I and III (Velling et al., 2002) and fibrillins (Kinsey et al., 2008). In the case of fibrillin-1, FN-dependent microfibril nucleation enhances TGFβ signaling (Ramirez and Rifkin, 2009 and references therein). In the context of angiogenic blood vessel remodeling, FN fibrils provide a platform for angiogenic signaling by increasing the bioavailability of diffused factors such as vascular endothelial growth factor (VEGF) and heparin-binding growth

factor 2 (FGF2) (Bossard et al., 2004; Wijelath et al., 2006). Several studies have shed light on the molecular mechanisms that underlie the polymerization of FN in vitro and in vivo (for reviews, see Leiss et al., 2008; Mao and Schwarzbauer, 2005). FN fibrillogenesis is a complex stepwise cell-driven process that takes place at specialized integrin-based structures called fibrillar adhesions on cell surfaces (Ohashi et al., 2002; Pankov et al., 2000; Zamir et al., 2000). Studies from our and other laboratories have demonstrated a clear role for the β-integrin effector integrin-linked protein kinase (ILK) and its partners in the formation of fibrillar adhesions and assembly of FN (Stanchi et al., 2009; Vouret-Craviari et al., 2004; Wu, 2004; Wu et al., 1998). Initial attempts to determine whether the fibrillogenesis defect could account for the phenotypic alterations of ILK-deficient endothelial cells led us to uncover the importance of autocrine FN in subendothelial FN matrix assembly and to investigate the cellular function of the cFN variants FN-EDB and FN-EDA by using isoform-specific RNA interference (RNAi).

Results

Cell-autonomous FN fibrillogenesis on the subendothelial cell surface

Cultured bovine aortic endothelial (BAE) cells are FN-producing cells that, similar to their in vivo counterparts, form polarized monolayers. After plating, BAE cells assemble α5-rich fibrillar adhesions and associated extracellular FN fibrils on their basal surface, as shown in Fig. 1A. Addition of basement membrane components (i.e. Matrigel) to the apical surface of cells rapidly disrupts organized cell monolayers and initiates the formation of primitive capillary-like structures ensheathed with FN (Fig. 1B). Time-course analyses of FN assembly (data not shown) suggested that fibril assembly is coupled to the basally oriented vectorial secretion of fibronectin previously documented in these cells (Unemori et al., 1990). Interestingly, following siRNA-mediated inhibition of FN production by cells, virtually all of the cell-associated FN fibrils were absent (Fig. 1C). In fact, all of the extracellular microfibrils detected by scanning electron microscopy beneath control cells disappeared following FN silencing (Fig. 1C, lower panels), suggesting that FN is the principal component of the subendothelial matrix of cultured BAE cells or at least that its presence is required for the assembly of other matrix proteins. The addition of high concentrations of soluble FN (up to 400 μg/ml) to FN-depleted cell monolayers did not restore the control phenotype (Fig. 1C), even when the plasma FN was presented to the basal surface of cells plated on permeable filters (data not shown), indicating that FN fibrillogenesis in BAE cells is a cell-autonomous process that requires endogenous production of the matrix protein. It is noteworthy that FN-deficient BAE cells were able to remodel plasma FN when presented in an active, extended conformation (i.e. adsorbed on glass coverslips). Although FN fibrillogenesis has been found to proceed in an RGD-independent manner (Sechler et al., 2000; Takahashi et al., 2007; Yang et al., 1993), α5β1 appears to be the sole integrin supporting this function in BAE cells as silencing of the α5 integrin subunit totally precluded FN assembly (see supplementary material Fig. S3B).

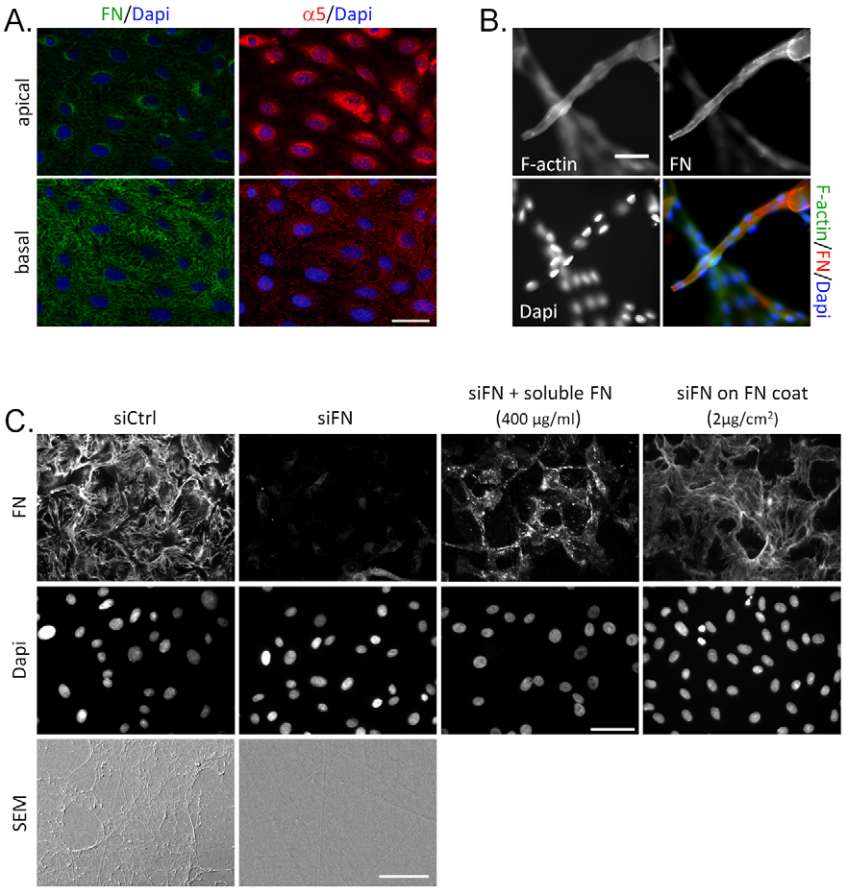

Fig. 1. Basal assembly of cell-produced FN by BAE cells. (**A**) Twenty-four hours after plating, BAE cells were stained for integrin α5 and FN. Confocal images were taken in both apical and basal planes (scale bar, 20 μm). (**B**) Cells were seeded on glass coverslips and, 24 h after adhesion, they were overlaid with a thin layer of Matrigel. Capillary-tube-like structures were visualized by fluorescence staining of F-actin, FN and nuclei (DAPI) (scale bar, 50 μm). (**C**) Control and FN-siRNA-transfected cells were fixed 24 h after plating and stained for FN. FN-deficient cells were plated in culture medium containing the indicated concentration of soluble plasma FN or plated on the indicated concentration of adsorbed plasma FN (scale bar, 50 μm). The ECM of control and FN knockdown cells, prepared as indicated in the Materials and Methods section, was visualized by scanning electron microscopy (scale bar, 5 μm).

Selective silencing of cellular FN variants produced by BAE cells

As previous studies have highlighted functional differences between locally produced cFN and circulating plasma FN, we turned our attention to the different FN variants produced by BAE cells (schematized in Fig. 2A). By RT-PCR analysis, we detected the presence of FN spliced variants containing either one (EDB or EDA), or both (EDB and EDA), exons (Fig. 2B). FN transcripts, lacking both EDB and EDA sequences, were undetectable in these cells.

For functional analyses, selective depletion of EDB- or EDA-containing transcripts was achieved by RNA interference (Fig. 2C). The effects were confirmed with two or more different siRNA sequences (supplementary material Fig. S1). Importantly, silencing of one or the other transcript had no significant impact on the levels of the remaining transcript. Western blotting of cell lysates with an antibody against total FN (Fig. 2D) revealed that depletion of either the EDB- or the EDA-containing variant induced a 40% decrease in the remaining FN levels. A similar pattern was observed for FN secreted into the medium by transfected cells (approximately 1.8 μg/ml for control cells and 1 μg/ml for variant-depleted cells, quantified by western blotting using plasma FN as a standard). Efficient reduction in EDA-containing protein levels was confirmed using an antibody against EDA; however, we were unable to specifically detect the EDB-containing variant using any of the antibodies tested. Given the fact that BAE cells do not express FN transcripts devoid of both extra domain sequences, we conclude that the total FN antibody recognizes the FN-EDB variant in EDA-depleted cells and the FN-EDA variant in EDB-depleted cells (Fig. 2E). Control and EDA-deficient cells displayed a more branched fibrillar network, compared with EDB-depleted cells, and no FN fibrils were detected following double knockdown of EDB and EDA (data not shown). Altogether, the results for protein expression, together with PCR quantification of transcript levels, indicate that EDA-depleted cells are attached to a FN-EDB matrix, and EDB-depleted cells adhere to a matrix comprising FN-EDA fibrils.

Table 1. Cell cycle analysis of siRNA-transfected cells

	siCtrl (%)	siFN (%)	siEDB (%)	siEDA (%)
SubG1	1.2	1.7±1.2	2.1±1.3	3.9±3.4
G1	54.2±1.1	*74.3±1.6	61.1±1.2	48.2±1.7
S	16.6±2.8	*7.4±1	13±1.6	13.2±0.6
G2–M	27.9±4.1	*16.7±3.9	23.9±4.1	*34.6±6.1

Depletion of fibronectin (FN) arrests cells in G1 phase. Eight hours after the second transfection, cells were plated on plastic. Twenty-four hours later, the still exponentially growing cells were trypsinized and stained with propidium iodide. Intensity was measured by flow cytometry. Results correspond to the means ± s.d. from three independent experiments (*P<0.05) compared with the control transfectants (siCtrl).

Depletion of FN increases G1 phase accumulation

To analyze the influence of the expression of FN variants on cell proliferation, we performed cell cycle analyses of exponentially growing siRNA-transfected cells (Table 1). In comparison with control cells, silencing of total FN led to an increase in G1 (74% versus 54%) and a decrease in S phase transit (7% versus 16%). Although deleting the EDB region resulted in a slight increase in G1 (61% versus 54%), EDA knockdown had no significant impact on G1 or S phase proportions, and it only slightly enhanced the number of cells in G2 (35% versus 28%). These results, together with cell counts from transfected populations (data not shown), indicate that FN production enhances growth. Although the EDB- and EDA-deficient cells produce similar quantities of FN, siEDB cells display a significant increase in G1 compared with siEDA cells (P<0.05) and a slower growth rate (data not shown). Thus,

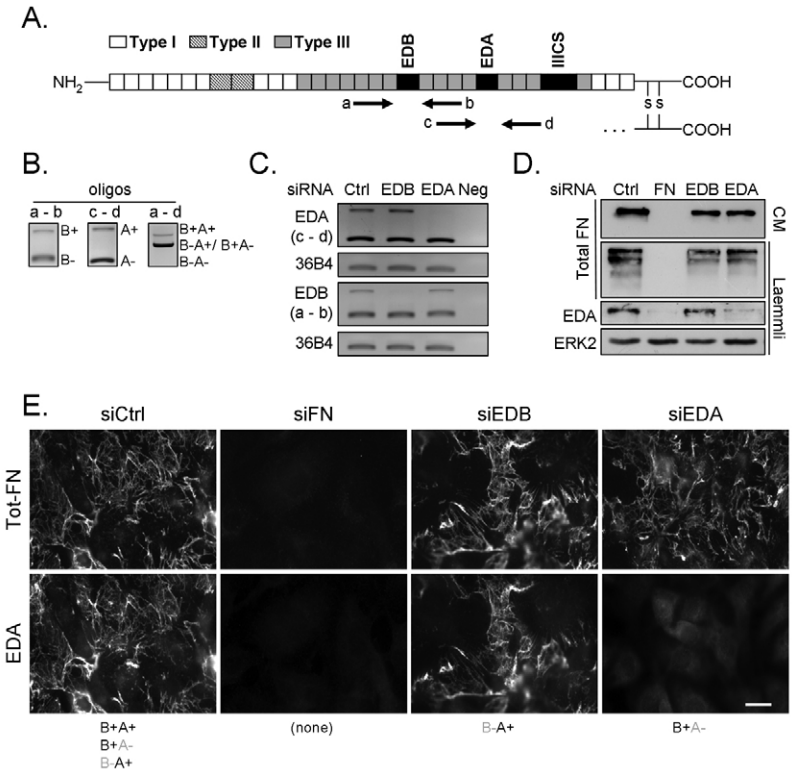

Fig. 2. Expression and selective knockdown of FN splice variants. (**A**) Schematic representation of the domain structure of FN. (**B**) FN variant expression levels in wild-type BAE cells, and (**C**) the knockdown efficiency of the extra regions or total FN determined by semi-quantitative RT-PCR on BAE cells using the oligos a, b, c and d, as indicated. (**D**) Total FN and FN-EDA variant protein levels in total lysates or conditioned medium were determined by western blotting. (**E**) Total FN and EDA-containing FN fiber organization was visualized by immunofluorescence (scale bar, 20 μm). FN variants present in the different conditions are indicated below the images.

EDB-deficient cells are less proliferative than cells lacking the EDA domain.

FN- and FN-EDB-depleted cells display a defect in capillary-like tube formation and increased scattering

Our previous studies of ILK function in BAE cells showed that ILK deficiency reduced intercellular cohesion in an in vitro capillary morphogenesis assay (Vouret-Craviari et al., 2004). To determine whether this could be accounted for by the defect in FN fibrillogenesis observed following ILK silencing, we examined the effect of total or isoform-specific FN silencing on capillary morphogenesis on Matrigel beds. As shown in Fig. 3A, FN-deficient cells phenocopied ILK-deficient cells. Similarly, EDB-depleted cells were incapable of forming multicellular alignments, suggesting that FN fibrils containing the EDB region promote cohesive interactions among neighboring cells. A similar alteration in cell cohesion was observed when cells were plated under sparse conditions on plastic culture dishes. Hence, migrating FN- and EDB-depleted endothelial cells remained dispersed, whereas control and EDA-depleted cells clung together upon collision.

FN and EDB depletion increases BAE cell motility and alters cytoskeletal organization

We next examined the motility of the different transfectants in cell tracking experiments. Under sparse conditions, FN- and EDB-depleted cells displayed a significant increase in the rate and directional persistence of their migration, as compared with control or EDA-depleted cells (Fig. 3). Thus, cells that do not express FN, or those that express only the FN-EDA variant, migrate nearly twice as far before changing the angle of their direction and therefore explore a greater surface than control or EDA-deficient cells. Increased chemotactic migration towards serum was observed in all of the FN-deficient cells with respect to control cells, with the EDB-depleted cells displaying the highest mobility (data not shown). It is noteworthy that both EDB- and EDA-deficient cells produce similar amounts of FN, so the altered motility of EDB-deficient cells under sparse conditions is more likely due to the nature of the FN variant secreted rather than the amount of FN.

The observed changes in the motile behavior of the cells were accompanied by morphological alterations that were most striking at early times during adhesion (Fig. 4A). Whereas control cells spread with a ‘fried egg’ morphology characterized by large cortactin-enriched lamellipodia and prominent stress fibers, FN-depleted cells displayed a uniaxial phenotype with small protrusions at opposite ends of the cells and dramatically reduced microfilament assembly. Consistent with their limited lamellipodial extensions and lack of F-actin bundles, FN-depleted cells displayed decreased levels of active Rac1 and RhoA GTPases, as determined by pulldown assays on exponentially growing cells (Fig. 4C). A spreading defect was also detected in EDB-depleted cells, albeit less severe than the FN-deficient cells, as silenced cells extended multiple protrusions (Fig. 4B). EDA-deficient cells spread in a manner similar to that of control cells. Altogether, these differences in cell spreading and locomotion indicate that cFN variants trigger distinct signals to the migration machinery and/or the steering mechanism of endothelial cells and suggest that cFN–integrin signaling might occur in an intracrine fashion.

Autocrine FN dictates cell–matrix adhesion

Cytoskeletal remodeling and cell migration depend on the assembly and disassembly of integrin-based adhesive structures. Spreading

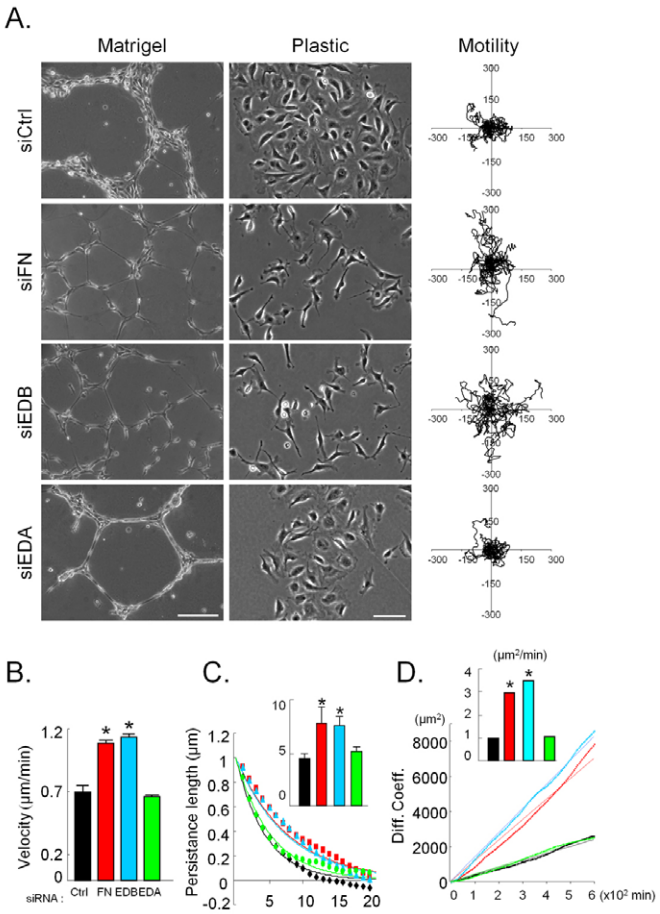

Fig. 3. FN-EDB- and total FN-depleted cells are less cohesive and more motile. (**A**) siRNA-treated cells were plated on either a thin layer of Matrigel or plastic 24 h after the second transfection. Images were taken 20 h after plating (scale bars, 200 µm). Cell movements on plastic were followed for 10 h and plotted on an *x*–*y* axis. One representative experiment is shown involving the analysis of 12 cells. Image analysis is detailed in the Materials and Methods section. (**B**) Mean velocity was quantified for control (black), FN (red), EDB (blue) and EDA (green) siRNA-transfected cells. Speed variation fitted well with a Poissonian distribution model (R^2>0.91) (data not shown), yielding results that are indistinguishable from the mean value of experimental speed measurements. (**C**) The experimental turning angle correlation curves (points) were fitted with a model (curves) to evaluate the distance of persistent migration (histogram). (**D**) Similarly, mean square displacement values (points) were fitted (curves) to extract diffusion coefficients (histogram). Error bars on histograms represent confidence intervals of 95% obtained from the fit parameters. Significant differences from the control are indicated (*).

is guided by nascent adhesions and small focal complexes at the cell periphery that are rich in αvβ3 integrin and tyrosine-phosphorylated proteins. Traction occurs at somewhat larger focal adhesions that associate with actin stress fibers, and assembly of the extracellular FN matrix takes place at long fibrillar adhesions characterized by their more central location and the presence of tensin and α5β1 integrin (Balaban et al., 2001). In an attempt to understand the observed differences in cohesion, migration and cytoskeletal organization among the transfectants, we next examined cell adhesion and localization of the predominant fibronectin-binding integrins in BAE cells. Twenty-four hours after plating on uncoated glass coverslips, control cells display numerous α5β1-rich fibrillar adhesions beneath extracellular FN fibrils

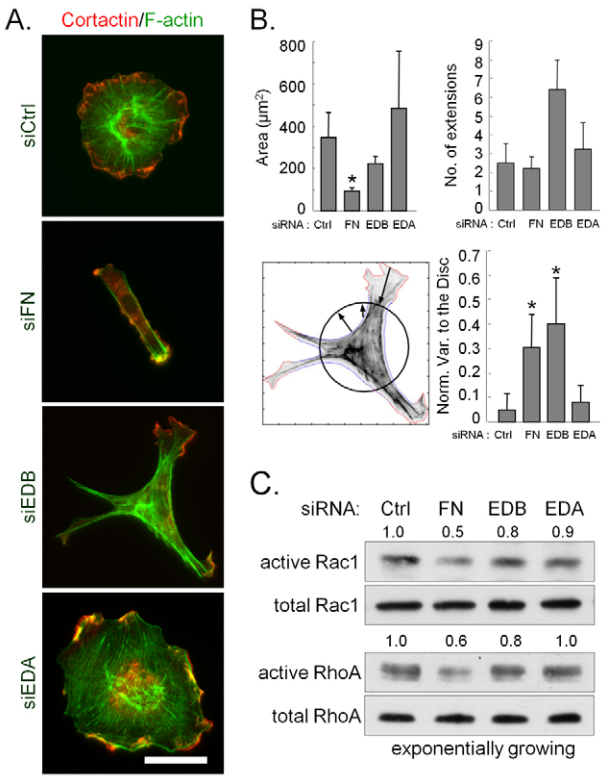

Fig. 4. Depletion of cFN variants alters cell morphology and GTPase activation. (**A**) Twenty-four hours after the second transfection, cells were plated on glass coverslips for 2.5 h, fixed and stained for F-actin (green) and cortactin (red). Scale bar: 20 μm. (**B**) Morphological analyses based on cell contour determinations were performed on 10–12 cells using software that distinguished extensions and retractions, as illustrated in B (bottom left). Mean cell area (top left), number of extensions per cell (top right) and normalized variance to the disk (bottom right) are shown. Details of the quantifications are indicated in the Materials and Methods section. Error bars represent the s.d. Analysis of variance was performed with ANOVA ($P<0.05$); values are significantly different from those of the control where indicated (*). (**C**) The levels of active RhoA and Rac1 were determined on exponentially growing cells harvested 24 h after plating.

(Vouret-Craviari et al., 2004) (Fig. 5A), whereas β3-staining is largely dispersed (Fig. 5A). A similar pattern was observed in EDA-deficient cells (attached to FN-EDB-containing fibrils). Not surprisingly, in total-FN-depleted cells (devoid of a subendothelial FN matrix), fibrillar adhesions were absent and α5 integrin staining was mainly diffuse. In these cells, short β3 integrin-based focal adhesions, presumably bound to adsorbed serum vitronectin, were abundant. Interestingly, EDB-depleted cells (attached to FN-EDA-containing fibrils) formed both focal (β3-based) adhesions and α5β1 fibrillar adhesions.

Hence, modifying cFN expression affects integrin usage. The adhesive function of the αvβ3 was confirmed in these cells using αv-integrin antagonists. As shown in Fig. 5A (right panel), cells displaying increased β3 integrin adhesions are more susceptible to detachment with αv integrin antagonists. Twenty hours after addition of antagonist to freshly plated cells, 73% of the FN-depleted cells and 51% of the EDB knockdown cells were round and detached, whereas the antagonist had little effect on the spreading of control or EDA-silenced cells.

Modification of integrin usage in turn modified integrin surface expression. Thus, expression of non-liganded α5β1 integrins on the surface of FN siRNA-transfected cells was 1.7-fold higher than control siRNA-transfected cells, as determined by FACS analysis (Fig. 5B), whereas the total levels of α5 and β1 subunits present in cell lysates did not vary (Fig. 5C). An increase in surface expression of αvβ3 was also detected following knockdown of either of the spliced FN variants.

It is well established that different adhesion receptors organize distinct signaling platforms and recruit different cytoskeletal-linking components to the cytoplasmic surface of the plasma membrane. In control BAE cells, ILK predominantly associated with α5 (data not shown) and tensin 1 in fibrillar adhesions (Fig. 5D). As previously reported, (Vouret-Craviari et al., 2004), paxillin is also present in these cell–matrix adhesions Interestingly, in FN-depleted cells, ILK together with the fibrillar adhesion marker tensin 1 (Geiger et al., 2001) was localized in short focal adhesions that colocalized with β3 integrin, and active β1 integrin was absent from adhesive structures (Fig. 5D, and data not shown). Thus, altering the ECM by FN depletion shifted ILK association from β1 to β3 integrins. These results demonstrate that autocrine cFN expression directs adhesion formation, the recruitment of intracellular effectors and presumably downstream signaling events. It is noteworthy that paxillin and, more markedly, phospho-tyrosine staining was enriched at sites of cell–cell adhesion in control cells, whereas only punctate staining in focal adhesions could be detected in FN-depleted cells (Fig. 5D).

FN–α5β1-integrin signaling regulates cell–cell adhesion

As cFN depletion results in decreased cell cohesion, we next determined the ability of the subendothelial FN matrix to impact on intercellular contacts. At confluence, control cells form a monolayer of closely apposed and nondividing cells in which adherens junctions can be clearly visualized by staining of the junctional components VE-cadherin, β-catenin and ZO-1 (Fig. 6; supplementary material Fig. S2). EDB- and the EDA-depleted cells formed cobblestone arrays upon confluence as well (data not shown). By contrast, FN depletion totally precluded the establishment of cell–cell junctions and the formation of apparently polarized monolayers in FN siRNA-transfected cells without affecting VE-cadherin levels (Fig. 6; supplementary material Fig. S2). Thus, upon confluence, FN-depleted cells were insensitive to contact inhibition of motility, and they continued to migrate above and below each other, as seen in the phase-contrast and scanning-electron micrographs of Fig. 6A (left) and in cell tracking experiments (Fig. 6A, middle; supplementary material Movies 1 and 2). Contact inhibition of cell growth was also impaired following FN depletion. As shown in Fig. 6A, we noted an increased saturation density in confluent cultures of FN-depleted cells in comparison with control cells. In addition, levels of pERK failed to decline at confluence, consistent with a loss of a contacted-inhibited state, as described by Wayne and colleagues (Wayne et al., 2006). From these results, together with the fact that depletion of α5β1 integrin (silencing of α5) similarly perturbed monolayer organization (supplementary material Fig. S3A), we conclude that the signaling through the subendothelial FN–α5β1 axis can promote endothelial monolayer integrity. Indeed, plating FN-depleted cells on a coat of absorbed plasma FN matrix, or coculturing them with cFN-producing cells, restored adherens junctions (Fig. 6B, middle; supplementary material Fig. S4A), whereas plating them on vitronectin was not competent for this effect (data not shown).

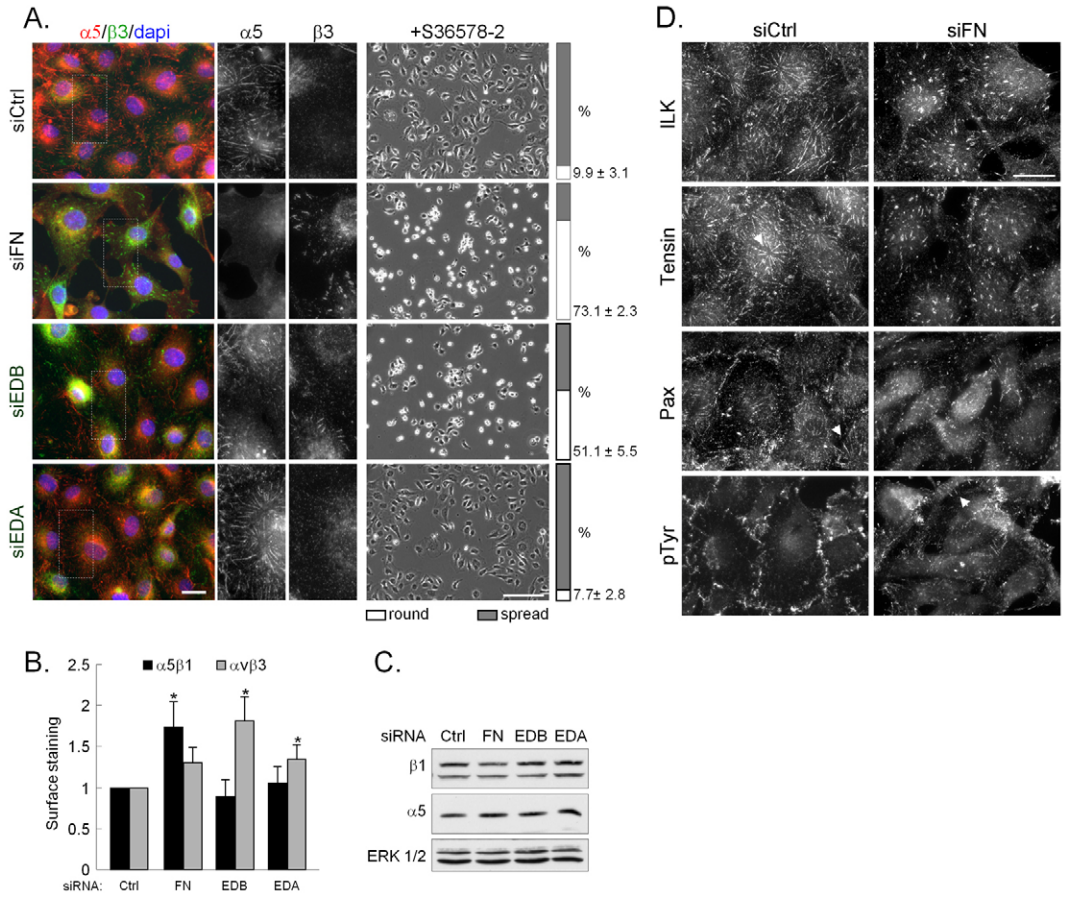

Fig. 5. Integrin adhesions in cells lacking cFN or the cFN variants. (**A**, left) Cells grown on glass coverslips for 24 h were fixed and stained for α5 (green) and β3 (red) integrin (scale bar, 20 μm). (A, right) The αv antagonist S36578-2 (5 μM) was added to subconfluent cells 2 h after plating. Images were taken after 20 h (scale bar, 200 μm). The proportion of round and spread cells was determined from six images per condition. Data from one representative experiment are shown. (**B**) The cell surface expression of α5β1 and αvβ3 integrins (mean values ± s.d.) was determined on exponentially growing cells by FACS analysis (n=3, *P<0.05). (**C**) Protein levels of α5 and β1 integrins were determined by western blotting on total lysates collected 20 h after seeding. (**D**) The localization of the indicated adhesion markers was visualized by immunofluorescent staining 24 h after plating (scale bar, 20 μm).

Src-regulated crosstalk between cell–matrix and cell–cell adhesions

To understand better the integrin-dependent signaling events that underlie junctional integrity in BAE cells, we turned our attention to Src-family tyrosine kinases (SFKs). Earlier work has demonstrated that clustering of β3 integrins can selectively activate c-Src (Arias-Salgado et al., 2003; Huveneers et al., 2007). Other studies have established a role for SFKs in the regulation of endothelial barrier function, both in vitro and in vivo (see Dejana et al., 2008; Gavard, 2009). As shown in Fig. 6, pharmacological inhibition of SFKs with SU6656 efficiently restored adherens junctions in FN-depleted cells and reduced their motility, as determined by VE-cadherin staining and cell tracking experiments (Fig. 6B; supplementary material Movie 3). This effect occurred without affecting the organization of β3-based adhesions (supplementary material Fig. S4B). Conversely, expression of a constitutively primed form of Src (Src^{YF}-GFP) in control cells perturbed the establishment and maintenance of cellular junctions, as visualized by VE-cadherin staining (GFP-positive cells; Fig. 6C). Altogether, these findings highlight the role of the FN–α5β1 axis in junctional stability and point to a role for Src signaling in crosstalk between cell–ECM and cell–cell adhesions.

Discussion

Elucidating the precise mechanisms that underlie FN assembly and its role in endothelial cell behavior is important for determining rational strategies for more effective anti-antiangiogenic/anti-tumoral approaches. Selective silencing of FN in cultured vascular endothelial cells has allowed us to demonstrate that secretion of cFN and its basal assembly are tightly coupled processes that play an important role in the endothelial cell phenotype. Inhibition of autocrine FN in cultured BAE cells prevents a ‘mesenchymal-like to endothelial’ transition by preventing the formation of a contact-inhibited monolayer. Our findings highlight intrinsic differences in cytoskeletal organization and motility in cells that express different cFN isoforms. Finally, they reveal an important role for the cFN–α5β1 integrin axis in endothelial cell plasticity by regulating crosstalk between cell–matrix and cell–cell adhesions.

Basal assembly of autocrine FN

Previous studies have described vectorial secretion and basal assembly of FN in confluent BAE cell cultures (Birdwell et al., 1978; Kowalczyk et al., 1990; Unemori et al., 1990). Here, we show that autocrine FN, as opposed to exogenous soluble FN, is crucial for FN fibrillogenesis. In keeping with this finding and with a role for FN in orchestrating the microfibril assembly of other matrix proteins, FN-depleted cells fail to deposit a microscopically detectable fibrillar matrix on the substratum. Instead, they convert to a fibroblastoid morphology, suggesting that, in vascular endothelial cells, the FN matrix helps to establish and maintain an apical–basal asymmetry. Thus, downmodulation of cFN expression, in lieu of (or together with) inhibiting assembly, might have profound implications for blocking angiogenic blood vessel remodeling in a tumor setting. cFN is induced by various angiogenic stimuli, including hypoxia, glucose, TGF-β, stress (mechanical and oxidative) and endothelial growth factors such as VEGF and FGF (Herschman, 1991; Khan et al., 2005). Once polymerized, cFN not only provides an adhesive ligand for

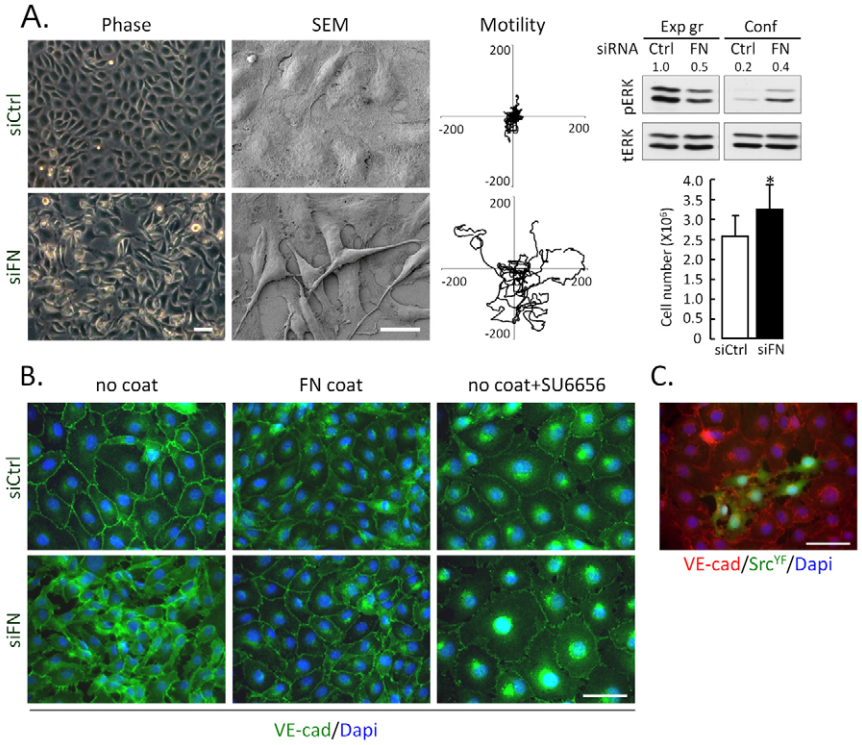

Fig. 6. cFN is necessary for the maintenance of cellular adhesions. (**A**) Phase contrast (scale bar, 25 µm) or scanning electron microscopy (scale bar, 20 µm) images of cells grown for 24 h on plastic. Cell tracking was performed on cells monitored for 10 h. The levels of total ERK (tERK) or phospho-ERK (pERK) were determined on cell lysates from exponentially growing cells or confluent monolayers. Cell counts were determined on confluent monolayers. (**B**) Cells were grown to confluence on glass coverslips and stained for VE-cadherin and DAPI (scale bar, 50 µm). Cells were plated on non-coated or coated (2 µg/cm^2 FN) coverslips for 12 h before adding, where indicated, the SFK inhibitor SU6656 (5 µM) for 12 h. (**C**) Control and Src^{YF}-GFP-expressing cells were fixed 24 h after plating, and VE-cadherin, GFP and nuclei (DAPI) were visualized by immunofluorescence (scale bar, 50 µm).

productive interaction with cellular receptors and matrix components, it also increases the bioavailability of angiogenic factors, including VEGF and FGF-2 (Bossard et al., 2004; Wijelath et al., 2006).

Role of FN variants

Previous studies on cultured cells have attributed a role for FN-EDB or EDA variants in adhesion, matrix assembly, dimer formation, secretion, differentiation and cell cycle progression (White et al., 2008 and references therein). These experiments have typically relied on the use of adsorbed cFN or recombinant FN peptides or fragments, and little attention has been paid to the importance of autocrine production or ligand topology in these effects. In addition to harboring additional integrin binding sites [α4β1 and α9β1, in the case of EDA (Liao et al., 2002; Pankov and Yamada, 2002)], inclusion of the extra domains has been suggested to introduce conformational modifications in the cell-binding domain that affect exposure of the RGD site (Balza et al., 2009; Carnemolla et al., 1992), thereby enhancing adhesive interactions. Here we show that control BAE cells assemble a FN matrix containing the EDB, EDA and EDB–EDA domains, whereas EDB- or EDA-depleted cells deposit FN-EDA or FN-EDB fibers, respectively. Although no major differences in fiber architecture were detected among the various isoforms, a noticeable reduction in the branching of FN-EDA fibers, compared with that of EDB-containing fibers, was observed. This difference is likely to reflect the increased rate and directional persistence of EDB-deficient cell migration, resulting from compromised signaling to the actin cytoskeleton. In light of the striking effect of EDB depletion on cytoskeletal organization and cell behavior, it will be interesting to examine the physical properties of the assembled isoforms more closely.

It is noteworthy that, following selective knockdown of either the EDB or EDA isoform, secreted and assembled FN levels amounted to 60% of control levels, despite the fact that single knockdowns also remove EDB–EDA-containing transcripts. This leads us to suggest that removing one variant of FN is compensated by increased production of the other. Consistent with our finding that BAE cells do not express transcripts that lack EDB and EDA, double silencing of EDB and EDA variants totally abrogates FN production and network formation (data not shown). These observations might explain why mice with deletions of EDA or EDB are viable (Fukuda et al., 2002; Muro et al., 2003) and display no major deficiencies in physiological or tumor angiogenesis (Astrof et al., 2004), whereas mice with simultaneous knockout of both exons (Astrof et al., 2007) have an embryonic-lethal phenotype similar to that of FN-null animals (George et al., 1997), thus highlighting the importance of self-produced cFN for neovessel formation in vivo.

Although FN-deficient BAE cells are unable to assemble soluble FN, they are able to remodel plasma FN when adsorbed on a rigid support in an extended (partially active) conformation. This is similar to findings reported by Bae and colleagues using fibroblastic cells derived from FN-null mouse embryonic stem cells (Bae et al., 2004). In this case, FN-null cells were able to assemble exogenously added plasma FN when plated on adsorbed plasma FN or laminin (LN), but not when plated on vitronectin. Thus, the nature of the substrate can play a permissive or suppressive role in FN assembly and thereby regulates the coupling of cFN expression and assembly in an in vivo setting.

Altered expression of FN splice variants has marked effects on BAE cell morphology, migration and organization into cord-like structures on Matrigel beds. The most striking effects occur following FN or EDB depletion. Although no EDB-specific cellular receptor has been identified to date, the EDB domain has been proposed to generate a conformational modification of the cell-binding domain of FN and improve the access to nearby integrin-binding domains (Hashimoto-Uoshima et al., 1997; Bencharit et al., 2007). Indeed, our data are consistent with a model in which

the inserted EDB segment serves to poise the ligand for productive α5β1 adhesive interactions and increased actomyosin contractility associated with this integrin. Interestingly, the defect in pseudocapillary formation on Matrigel is phenocopied by ILK-deficient BAE cells, which display a severe FN fibrillogenesis defect (Vouret-Craviari et al., 2004). Based on these results, we propose that a pericellular FN matrix containing the EDB domain might promote efficient capillary morphogenesis in endothelial cells. It is likely that defective FN fibrillogenesis underlies some of the phenotypic abnormalities observed in ILK-null mice (for a review, see McDonald et al., 2008). Consistent with our model, Zhou and colleagues (Zhou et al., 2008) reported that endothelial cells initiate neovascularization by unfolding soluble FN and depositing a network of fibrils that regulate cytoskeletal organization and acto-myosin contractility. However, in that study, FN matrix assembly was monitored by incorporation of fluorescent plasma FN, and the importance of autocrine FN was not evoked.

As for the function of FN containing the EDA FN type III repeat, we did not observe major morphological or behavioral effects in BAE cells following its removal. Hence, this variant might not be essential for autocrine functions in vascular endothelial cells if FN-EDB is present. Instead, FN-EDA might promote angiogenesis through paracrine mechanisms by providing binding sites for the recruitment of α4β1- and α9β1-expressing cells, including bone-marrow-derived cells and mural cells (see Avraamides et al., 2008; White et al., 2008). By contrast, the FN-EDA-α9β1 integrin interaction was recently found to regulate FN assembly in primary cultured human lymphatic endothelial cells and to be required for lymphatic valve morphogenesis in vivo (Bazigou et al., 2009). In this case, fibril assembly is RGD independent. It will be of interest to elucidate further the molecular mechanisms underlying α9β1-driven FN fibrillogenesis.

FN- and EDB-depleted cells share a similar non-cohesive phenotype. They migrate faster and explore a greater territory than control or EDA-deficient cells, consistent with their being less tethered to the substratum. Differences in cell spreading can be observed as early as 2.5 h after adhesion (i.e. before the initiation of fibrillogenesis in cFN-producing cells); thus, it is tempting to speculate that cFN expression triggers intracrine signaling events in these cells. Efficient cell spreading requires membrane-protrusive activity and effective stabilization of nascent adhesions at the edge of lamellipodia. Indeed, we observe differences in the adhesive structures formed by the various transfectants. In all cells, initial adhesion occurs through integrin αvβ3 (data not shown). Thereafter, production and assembly of cFN induces the appearance of fibrillar α5β1 integrin adhesions. However, in the absence of a cFN matrix, cells are unable to perform this switch and they remain attached through αvβ3 adhesions, totally sensitive to detachment by an αv antagonist. Interestingly, EDB-deficient cells, on a FN-EDA matrix, engage both αvβ3 and α5β1 integrins. Thus, the dynamic modulation of integrin usage should be taken into consideration when considering the anti-angiogenic effects of αv integrin antagonists or the design of more effective anti-angiogenic agents.

Previous studies in epithelial cells and fibroblasts have demonstrated that directionality of migration is dependent on specific integrin usage and recycling (Danen et al., 2005; Roberts et al., 2001; White et al., 2007; Woods et al., 2004). Thus, cells predominantly adhering through integrin α5β1 (shuttled by Rab11 perinuclear endosomes) have increased RhoA activity that decreases cofilin phosphorylation and eventually leads to random migration. Conversely, when αvβ3 is used [shuttled by Rab4 and the serine/threonine-protein kinase D1 (PRKD1) in early endosomes], RhoA activation decreases, cofilin increases and the persistence of cell migration increases. Our observations are consistent with these findings, as siFN and siEDB cells that are completely or partially dependent on αvβ3 adhesion exhibit an increased directional migration that is coupled to a major or mild decrease in RhoA activity, respectively. Receptor recycling pathways transport integrins forward in migrating cells (Bretscher, 1996). Perturbing the fast Rab4-dependent recycling of αvβ3 increases the Rab11-dependent α5β1 recycling and vice versa (White et al., 2007). Deleting total FN or the EDB-including variants differentially affects integrin recycling. Despite the increased, but diffuse, surface expression of α5β1 in FN-depleted cells, only the clustered and active αvβ3 integrins transmit the extracellular signals. EDB-depleted cells increase their αvβ3 surface expression, probably by interfering with α5β1 recycling, which could account for the increased persistence of directional migration observed.

The subendothelial cFN matrix and endothelial plasticity

Our findings in cultured endothelial cells that FN-deficient cells lose their intercellular adhesions and contact inhibition are reminiscent of an endothelial-to-mesenchymal transition and consistent with a model in which the cFN plays a key role in endothelial integrity by controlling the establishment and maintenance of adherens and tight junctions. We show here that cross-talk between cell–matrix and cell–cell adhesion in BAE cells is dependent on α5β1 and αvβ3 integrins and SFK signaling. This confirms and extends previous studies that demonstrate a role for the FN–α5β1 integrin axis in cell polarity in *Xenopus* and zebrafish (Koshida et al., 2005; Marsden and DeSimone, 2001; Trinh and Stainier, 2004). Loss of ZO-1 junctional staining in FN-deficient BAE cells is compatible with the fact that genetic ablation of mouse ZO-1 leads to defects similar to those observed in FN-null embryos (Katsuno et al., 2008). In contrast to the rescue obtained

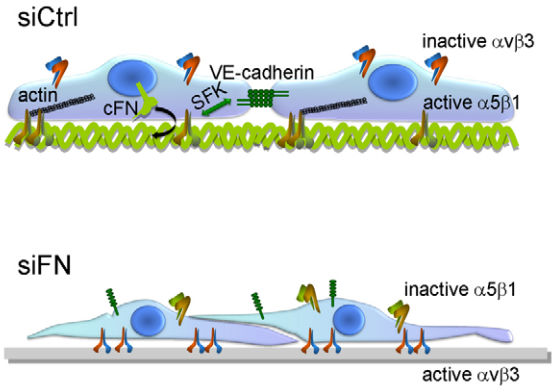

Fig. 7. Schematic representation of autocrine FN regulation of cell–matrix and cell–cell adhesions. (**Top panel**) Autocrine FN is secreted basally and assembled at α5β1 integrin-based fibrillar adhesions, thereby providing apico-basal polarity cues and promoting the establishment and maintenance of VE-cadherin-based adherens junctions in confluent endothelial monolayers. Crosstalk between cell–matrix and cell–cell adhesion is regulated by SFKs. (**Bottom panel**) In the absence of a subendothelial FN matrix (siFN), αvβ3 integrin adhesion prevails, SFK activity increases, non-liganded α5β1 integrin accumulates at the cell surface and cells fail to establish a polarized monolayer with VE-cadherin localized in adherens junctions.

by α5β1 integrin activation, we were unable to restore cellular junctions in FN-depleted cultures by plating them on vitronectin-coated surfaces (αvβ3 integrin adhesion) or by pharmacological activation of Rap1, a GTPase previously shown to regulate adhesion and junction formation in endothelial cells (Carmona et al., 2009; Kooistra et al., 2007) (data not shown). In agreement with reports that inhibition of SFKs can stabilize endothelial cell junctions (Paul et al., 2001; Scheppke et al., 2008; Weis et al., 2004), addition of the SFK inhibitor SU6656 re-established cellular junctions. Accordingly, control cells expressing a constitutively primed Src^{YF}-GFP construct were unable to establish cell–cell adhesions. From these data, we conclude that the absence of the FN matrix in endothelial cells results in loose adherence through αvβ3 integrins. The presence of αvβ3 signaling enhances SFK activity, which in turn precludes the formation and maintenance of cellular junctions. Our results allow us to propose a novel model in which cFN expression and cell-autonomous matrix assembly controls endothelial plasticity following angiogenic stimulation by coordinating α5β1 integrin and SFK-dependent regulation of cell–cell and cell–matrix interactions, as schematized in Fig. 7.

Materials and Methods

Materials

All reagents were of the highest grade commercially available. The non-peptidic αv integrin antagonist (S36578-2) kindly provided by G. Tucker and J. Hickman (Institut de Recherches Servier, Croissy sur Seine, France) has been described previously (Maubant et al., 2006). The Src inhibitor SU6656 was purchased from Merck4Biosciences (Nottingham, UK). Human plasma fibronectin was purchased from BD Bioscience (Le Pont De Claix, France) and human cellular fibronectin was purchased from Sigma (St Quentin Fallavier, France). Tissue-culture plasticware was from Nunc (Roskilde, Denmark) and Falcon (BD Biosciences, San Diego, CA), for time-lapse analysis.

Cell culture

BAE cells have been described previously (Vouret-Craviari et al., 2004). For collection of conditioned media, cells (2.5×10^5) were seeded in 100 mm culture dishes 24 h after the second transfection with RNA duplexes. After 2 h, cells were washed in serum-free medium and then incubated for an additional 24 h in serum-free medium containing 0.1% bovine serum albumin (BSA). Conditioned medium was harvested and clarified by centrifugation.

Cell-derived matrix

Twenty-four hours after plating, cells were treated with 5 nM NH_4OH for 5 min at room temperature, then rinsed three times with water and fixed with 1% glutaraldehyde. Matrix was visualized by scanning electron microscopy.

siRNAs, double-stranded RNA transfection and retroviral infection

The constitutively active primed Src^{YF}-GFP construct, kindly provided by E. Danen (LACDR, Leiden, The Netherlands), has been reported previously (Huveneers et al., 2007). Transduction of BAE cells with the retroviral vector was performed as described (Boulter et al., 2006). Short interfering RNAs (siRNAs) were purchased from Eurogentec (Serang, Belgium). Equal amounts of complementary RNA oligonucleotides were combined to a final concentration of 20 μM and annealed according to the protocol supplied by the manufacturer. RNA interference in BAE cells was achieved by performing two transfections of double-stranded RNA, the first 7 h after plating and the second 24 h later, using a modified calcium-phosphate protocol. Unless otherwise stated, cells were analysed between 24 h and 48 h after the second transfection. The siRNA sequences used in this study to target EDA (5′-CAUUGAUCGCCCUAAAGGATT and 3′-TTGUAACUAGCGGGAUUUCCU), EDB (5′-GCAUCGGCCUGAGGUGGACTT and 3′-TTCGUAGCCGGACUCCACCUG), FN (5′-ACAAUGGAGUGAACUACAATT and 3′-TTUGUUACCUCACUUGAUGUU) and α5 (5′-CUUCUCCAGCCUGAGCUGCTT and 3′-TTGCAGCUCAGGCUGGAGAAG) correspond to a region in the human gene encoding FN of identical sequence in bovine cDNA. Results were confirmed using one or more additional targeting sequences (see supplementary materials Fig. S1). As a control, an RNA duplex designed to target the *Drosophila* ILK transcript (GenBank accession number AF226669) was used (5′-CCCAAGCUCCGCAUCUUUUCTT and 3′-TTGGGUUCGAGGCGUAGAAAAG).

Semi-quantitative PCR

Total cellular RNA was extracted with the TRIzol reagent (Invitrogen, Cergy Pointoise, France). Reverse transcription PCR (RT-PCR) of 0.5 μg RNA was performed with the QIAGEN (Courtaboeuf, France) One-Step RT PCR kit. Forward and reverse primers used to flank the EDB region were respectively: 5′-CCTGGAGTACAATGTCAGTG-3′ and 5′-GGTGGAGCCCAGGTGACA-3′ and for the EDA region: 5′-GCAGCCCACAGTGGAGTAT-3′ and 5′-GGAGCAAGGTTGATTTCTTT-3′. Gene *36B4* was used as internal control (5′-GGCGACCTGGAAGTCCAACT-3′ and 5′-CCATCAGCACCACAGCCTTC-3′).

Antibodies

Anti-Rac1 monoclonal (clone 23A8), anti-α5 integrin subunit polyclonal (AB1928), anti-αvβ3 integrin monoclonal (MAB1976Z), anti-α5β1 integrin monoclonal (MAB1999), anti-FN polyclonal and the anti-phosphotyrosine monoclonal (clone 4G10) antibodies were purchased from Millipore (Billerica, MA). Anti-ILK (clone 65.1.9) and cortactin (clone AF11) monoclonal antibodies were from Upstate (Chemicon International, Hampshire, UK). Anti-RhoA (clone 26C4) monoclonal and anti-ERK1 (clone 16) polyclonal antibodies were from Santa Cruz Biotechnology (Santa Cruz, CA). The anti-FN (clone 10) and anti-paxillin monoclonal antibodies were from BD Biosciences (San Diego, CA), anti-EDA monoclonal (IST-9 and FN-3) was from Abcam (Cambridge, MA) and anti-phospho-ERK1/2 monoclonal from Sigma-Aldrich (St Louis, MO). Anti-VE-cadherin was from Bender MedSystems (Tebu-bio SA, Le Perray en Yvelines, France) and anti-β3 integrin subunit (Luc.A5) monoclonal antibody was purchased from Emfret (Eibelstadt, Germany). The anti-β1 integrin subunit and anti-tensin1 polyclonal antibodies were kindly provided by C. Albigez-Rizo (Institut Albert Bonniot, Grenoble, France) and S-H. Lo (University of California Davis, CA), respectively. Secondary antibodies coupled to horseradish peroxidase were from Promega France (Charbonnières-les-Bains, France). Fluorescently labeled secondary antibodies and phalloidin (Alexa Fluor 488, Alexa Fluor 546 and Alexa Fluor 647) were purchased from Invitrogen (Cergy Pointoise, France).

Western blotting and immunoprecipitation

Western blots were performed on whole-cell lysates or conditioned culture medium essentially as described previously (Vouret-Craviari et al., 2004). Immune complexes on membranes were detected by enhanced chemiluminescence (Pierce, Rockford, IL). Where indicated, immunoblots were quantified using the GeneGnome chemiluminescent imaging system (Syngene, Frederick, MD)

Immunofluorescence and microscopy

For immunofluorescence analyses, BAE cells plated on non-coated or coated glass coverslips with the indicated matrix protein were fixed in a solution of 3% paraformaldehyde containing 3% sucrose. Cells were permeabilized with 0.2% Triton X-100. After staining, the coverslips were mounted in ProLong Gold antifade reagent (Invitrogen). Fluorescence was observed through ×40 (1.3 NA), ×63 (1.4 NA) or ×100 (1.3 NA) oil objectives on a Zeiss inverted microscope (Axiovert 200M) equipped with a CoolSnap HQ cooled charge-coupled-device camera (Roper Scientifique, Evry, France). Phase-contrast and video microscopy were performed using a ×10 (0.25 NA) air objective. Image acquisition was performed using the MetaMorph Imaging System (Universal Imaging Corp., Downingtown, PA). Confocal microscopy was performed using a Zeiss LSM 510 META confocal laser scanning microscope. Cell-derived ECM for scanning electron microscopy was prepared by treating monolayers with 5 mM NH_4OH for 5 min at room temperature. Thereafter, samples were rinsed three times with water and fixed with 1.6% glutaraldehyde in 0.1 M phosphate buffer, washed and post-fixed in 1% osmium tetroxide in the same buffer. After washing with distilled water, the samples were dehydrated in a graded ethanol series, immersed in hexamethyldisilazane (Carl Roth, Karlsruhe, Germany), and dried at room temperature. The samples were mounted on aluminium stubs and sputter coated with gold–palladium (Cressington 308EM, UK). Examination was performed using a field emission scanning electron microscope (FESEM JEOL 6700F, Japan).

Image analysis

Image analysis was performed using MatLab (The MathWorks). Cell velocity was determined by manual tracking. From cell tracks, the turning angle was measured and its correlation function was calculated. The exponential fit of this function provides an estimation of persistence length, or the distance after which a cell changes its orientation (Petrie et al., 2009). Directionality was also determined from tracks by calculating the mean square displacement. Statistically, the mean square for Brownian movement on a plane surface is $\langle X^2\rangle=4Dt$ where t is time and D the diffusion coefficient. The linear behavior of the experimental curves confirms random walk properties of cell movement and allows the estimation of a diffusion coefficient, which represents the surface explored by the cell per time unit. The accuracy of the fits was verified by the R^2 value and the robustness of parameters extracted from the model was estimated by measuring the interval of confidence at 95%.

An application program was developed to describe cell morphology. From intensity threshold determinations, cell contour and curvature measurements were used to identify zones of extension and retraction. The number of extensions corresponds to the number of distinct regions of convex curvature. We used normalized variance to the disk (NVD) to estimate circularity, which was determined from cell contour by defining a disk with an area equivalent to that of

the cell and centered on the barycentre of the cell. Minimal distance $d_m(x)$ between the contour position and the circle was determined. Then, NVD was defined as the variance of $d_m(x)$ divided by the radius of the disk. Hence, the NVD is between 0 (circle) to 1 (star shaped).

Fluorescence-activated cell sorting

For cell cycle analysis, cells were lifted from the plates with a cell dissociation solution (Sigma-Aldrich), fixed with ethanol for 1 h at 4°C, washed with sodium citrate and then subjected to propidium iodide staining and fluorescence-activated cell sorting (FACS) analysis of DNA content using a FACScalibur (Becton Dickinson, Bedford, MA). Determination of cell-surface integrin expression has been described previously (Vouret-Craviari et al., 2004).

Migration assays and tube-like structure formation

For random migration, 10^4 BAE cells were plated in six-well plates. Cell movements were monitored for 10 h by time-lapse microscopy. Persistence of migration (distance from start / total migrated distance) and speed were determined using MetaMorph software. Chemotactic migration of BAE cells was analyzed on transwell filters as described previously (Vouret-Craviari et al., 2004). Six different fields of each transwell were photographed, and cells were counted using ImageJ software.

Capillary morphogenesis was analyzed as described previously (Vouret-Craviari et al., 2004) using Matrigel (Becton Dickinson) at concentrations between 9 and 12.5 μg/ml. The Matrigel overlay assay was performed as described previously (Connolly et al., 2002).

Determination of small GTPase activity

Determination of RhoA and Rac1 activity in exponentially growing BAE cells was determined as described previously in pulldown assays using GST-rhotekin and GST-PAK, respectively, (Boulter et al., 2006; Vouret-Craviari et al., 2004).

Coculture of control and FN-depleted cells

FN-depleted cells 24 h after transfection were stained with 1 μM carboxyfluorescein diacetate succinimidyl ester (CFSE) (Invitrogen) in PBS and 5% FCS for 5 min at room temperature. After staining, cells were rinsed three times with PBS and 5% FCS. The stained FN knockdown cells and control cells were plated together on coverslips in a 1:2 ratio, respectively. Cellular junctions and the colored FN-depleted cells were visualized by fluorescence microscopy 24 h after plating.

We thank Jean-Pierre Laugier and Pierre Gounon (Centre Commun de Microscopie Appliquée of the University of Nice-Sophia Antipolis) for performing the scanning electron microscopy. Elisabetta Dejana, Gordon Tucker and Fabio Stanchi are gratefully acknowledged for fruitful discussions and critical reading of the manuscript. Financial support for this work was provided by the CNRS-University of Nice-Sophia Antipolis (UMR6543), the Centre A. Lacassagne, the French National Institute of Cancer (INCa) and the Association of International Cancer Research. S.S. is affiliated to the PRISM Platform, UMR6543 CNRS/UNSA/IBDC and E.V.O.-S. is an INSERM investigator.

Supplementary material available online at
http://jcs.biologists.org/cgi/content/full/123/22/3989/DC1

References

Arias-Salgado, E. G., Lizano, S., Sarkar, S., Brugge, J. S., Ginsberg, M. H. and Shattil, S. J. (2003). Src kinase activation by direct interaction with the integrin beta cytoplasmic domain. *Proc. Natl. Acad. Sci. USA* **100**, 13298-13302.

Astrof, S. and Hynes, R. O. (2009). Fibronectins in vascular morphogenesis. *Angiogenesis* **12**, 165-175.

Astrof, S., Crowley, D., George, E. L., Fukuda, T., Sekiguchi, K., Hanahan, D. and Hynes, R. O. (2004). Direct test of potential roles of EIIIA and EIIIB alternatively spliced segments of fibronectin in physiological and tumor angiogenesis. *Mol. Cell. Biol.* **24**, 8662-8670.

Astrof, S., Crowley, D. and Hynes, R. O. (2007). Multiple cardiovascular defects caused by the absence of alternatively spliced segments of fibronectin. *Dev. Biol.* **311**, 11-24.

Avraamides, C. J., Garmy-Susini, B. and Varner, J. A. (2008). Integrins in angiogenesis and lymphangiogenesis. *Nat. Rev. Cancer* **8**, 604-617.

Bae, E., Sakai, T. and Mosher, D. F. (2004). Assembly of exogenous fibronectin by fibronectin-null cells is dependent on the adhesive substrate. *J. Biol. Chem.* **279**, 35749-35759.

Balaban, N. Q., Schwarz, U. S., Riveline, D., Goichberg, P., Tzur, G., Sabanay, I., Mahalu, D., Safran, S., Bershadsky, A., Addadi, L. et al. (2001). Force and focal adhesion assembly: a close relationship studied using elastic micropatterned substrates. *Nat. Cell Biol.* **3**, 466-472.

Balza, E., Sassi, F., Ventura, E., Parodi, A., Fossati, S., Blalock, W., Carnemolla, B., Castellani, P., Zardi, L. and Borsi, L. (2009). A novel human fibronectin cryptic sequence unmasked by the insertion of the angiogenesis-associated extra type III domain B. *Int. J. Cancer* **125**, 751-758.

Bazigou, E., Xie, S., Chen, C., Weston, A., Miura, N., Sorokin, L., Adams, R., Muro, A. F., Sheppard, D. and Makinen, T. (2009) Integrin-alpha9 is required for fibronectin matrix assembly during lymphatic valve morphogenesis. *Dev. Cell* **17**, 175-186.

Bencharit, S., Cui, C. B., Siddiqui, A., Howard-Williams, E. L., Sondek, J., Zuobi-Hasona, K. and Aukhil, I. (2007). Structural insights into fibronectin type III domain-mediated signaling. *J. Mol. Biol.* **367**, 303-309.

Birdwell, C. R., Gospodarowicz, D. and Nicolson, G. L. (1978). Identification, localization, and role of fibronectin in cultured bovine endothelial cells. *Proc. Natl. Acad. Sci. USA* **75**, 3273-3277.

Bossard, C., Van den Berghe, L., Laurell, H., Castano, C., Cerutti, M., Prats, A. C. and Prats, H. (2004). Antiangiogenic properties of fibstatin, an extracellular FGF-2-binding polypeptide. *Cancer Res.* **64**, 7507-7512.

Boulter, E., Grall, D., Cagnol, S. and Van Obberghen-Schilling, E. (2006). Regulation of cell-matrix adhesion dynamics and Rac-1 by integrin linked kinase. *FASEB J.* **20**, 1489-1491.

Bretscher, M. S. (1996). Moving membrane up to the front of migrating cells. *Cell* **85**, 465-467.

Carmona, G., Gottig, S., Orlandi, A., Scheele, J., Bauerle, T., Jugold, M., Kiessling, F., Henschler, R., Zeiher, A. M., Dimmeler, S. et al. (2009). Role of the small GTPase Rap1 for integrin activity regulation in endothelial cells and angiogenesis. *Blood* **113**, 488-497.

Carnemolla, B., Leprini, A., Allemanni, G., Saginati, M. and Zardi, L. (1992). The inclusion of the type III repeat ED-B in the fibronectin molecule generates conformational modifications that unmask a cryptic sequence. *J. Biol. Chem.* **267**, 24689-24692.

Connolly, J. O., Simpson, N., Hewlett, L. and Hall, A. (2002). Rac regulates endothelial morphogenesis and capillary assembly. *Mol. Biol. Cell* **13**, 2474-2485.

Danen, E. H., van Rheenen, J., Franken, W., Huveneers, S., Sonneveld, P., Jalink, K. and Sonnenberg, A. (2005). Integrins control motile strategy through a Rho-cofilin pathway. *J. Cell Biol.* **169**, 515-526.

Dejana, E., Orsenigo, F. and Lampugnani, M. G. (2008). The role of adherens junctions and VE-cadherin in the control of vascular permeability. *J. Cell Sci.* **121**, 2115-2122.

Ffrench-Constant, C. and Hynes, R. O. (1989). Alternative splicing of fibronectin is temporally and spatially regulated in the chicken embryo. *Development* **106**, 375-388.

Fukuda, T., Yoshida, N., Kataoka, Y., Manabe, R., Mizuno-Horikawa, Y., Sato, M., Kuriyama, K., Yasui, N. and Sekiguchi, K. (2002). Mice lacking the EDB segment of fibronectin develop normally but exhibit reduced cell growth and fibronectin matrix assembly in vitro. *Cancer Res.* **62**, 5603-5610.

Gavard, J. (2009). Breaking the VE-cadherin bonds. *FEBS Lett.* **583**, 1-6.

Geiger, B., Bershadsky, A., Pankov, R. and Yamada, K. M. (2001). Transmembrane crosstalk between the extracellular matrix-cytoskeleton crosstalk. *Nat. Rev. Mol. Cell Biol.* **2**, 793-805.

George, E. L., Georges-Labouesse, E. N., Patel-King, R. S., Rayburn, H. and Hynes, R. O. (1993). Defects in mesoderm, neural tube and vascular development in mouse embryos lacking fibronectin. *Development* **119**, 1079-1091.

George, E. L., Baldwin, H. S. and Hynes, R. O. (1997). Fibronectins are essential for heart and blood vessel morphogenesis but are dispensable for initial specification of precursor cells. *Blood* **90**, 3073-3081.

Glukhova, M. A., Frid, M. G., Shekhonin, B. V., Vasilevskaya, T. D., Grunwald, J., Saginati, M. and Koteliansky, V. E. (1989). Expression of extra domain A fibronectin sequence in vascular smooth muscle cells is phenotype dependent. *J. Cell Biol.* **109**, 357-366.

Hashimoto-Uoshima, M., Yan, Y. Z., Schneider, G. and Aukhil, I. (1997) The alternatively spliced domains EIIIB and EIIIA of human fibronectin affect cell adhesion and spreading. *J. Cell Sci.* **110**, 2271-2280.

Herschman, H. R. (1991). Primary response genes induced by growth factors and tumor promoters. *Annu. Rev. Biochem.* **60**, 281-319.

Huveneers, S., van den Bout, I., Sonneveld, P., Sancho, A., Sonnenberg, A. and Danen, E. H. (2007). Integrin alpha v beta 3 controls activity and oncogenic potential of primed c-Src. *Cancer Res.* **67**, 2693-2700.

Hynes, R. O. (2007). Cell-matrix adhesion in vascular development. *J. Thromb. Haemost.* **5**, 32-40.

Katsuno, T., Umeda, K., Matsui, T., Hata, M., Tamura, A., Itoh, M., Takeuchi, K., Fujimori, T., Nabeshima, Y., Noda, T. et al. (2008). Deficiency of zonula occludens-1 causes embryonic lethal phenotype associated with defected yolk sac angiogenesis and apoptosis of embryonic cells. *Mol. Biol. Cell* **19**, 2465-2475.

Khan, Z. A., Chan, B. M., Uniyal, S., Barbin, Y. P., Farhangkhoee, H., Chen, S. and Chakrabarti, S. (2005). EDB fibronectin and angiogenesis – a novel mechanistic pathway. *Angiogenesis* **8**, 183-196.

Kinsey, R., Williamson, M. R., Chaudhry, S., Mellody, K. T., McGovern, A., Takahashi, S., Shuttleworth, C. A. and Kielty, C. M. (2008). Fibrillin-1 microfibril deposition is dependent on fibronectin assembly. *J. Cell Sci.* **121**, 2696-2704.

Kooistra, M. R., Dube, N. and Bos, J. L. (2007). Rap1: a key regulator in cell-cell junction formation. *J. Cell Sci.* **120**, 17-22.

Koshida, S., Kishimoto, Y., Ustumi, H., Shimizu, T., Furutani-Seiki, M., Kondoh, H. and Takada, S. (2005). Integrinalpha5-dependent fibronectin accumulation for maintenance of somite boundaries in zebrafish embryos. *Dev. Cell* **8**, 587-598.

Kowalczyk, A. P., Tulloh, R. H. and McKeown-Longo, P. J. (1990). Polarized fibronectin secretion and localized matrix assembly sites correlate with subendothelial matrix formation. *Blood* **75**, 2335-2342.

Leiss, M., Beckmann, K., Giros, A., Costell, M. and Fassler, R. (2008). The role of integrin binding sites in fibronectin matrix assembly in vivo. *Curr. Opin. Cell Biol.* **20**, 502-507.

Liao, Y. F., Gotwals, P. J., Koteliansky, V. E., Sheppard, D. and Van De Water, L. (2002). The EIIIA segment of fibronectin is a ligand for integrins alpha 9beta 1 and alpha 4beta 1 providing a novel mechanism for regulating cell adhesion by alternative splicing. *J. Biol. Chem.* **277**, 14467-14474.

Mao, Y. and Schwarzbauer, J. E. (2005). Fibronectin fibrillogenesis, a cell-mediated matrix assembly process. *Matrix Biol.* **24**, 389-399.

Marsden, M. and DeSimone, D. W. (2001). Regulation of cell polarity, radial intercalation and epiboly in Xenopus: novel roles for integrin and fibronectin. *Development* **128**, 3635-3647.

Maubant, S., Saint-Dizier, D., Boutillon, M., Perron-Sierra, F., Casara, P. J., Hickman, J. A., Tucker, G. C. and Van Obberghen-Schilling, E. (2006). Blockade of alpha v beta3 and alpha v beta5 integrins by RGD mimetics induces anoikis and not integrin-mediated death in human endothelial cells. *Blood* **108**, 3035-3044.

McDonald, P. C., Fielding, A. B. and Dedhar, S. (2008). Integrin-linked kinase-essential roles in physiology and cancer biology. *J. Cell Sci.* **121**, 3121-3132.

Muro, A. F., Chauhan, A. K., Gajovic, S., Iaconcig, A., Porro, F., Stanta, G. and Baralle, F. E. (2003). Regulated splicing of the fibronectin EDA exon is essential for proper skin wound healing and normal lifespan. *J. Cell Biol.* **162**, 149-160.

Neri, D. and Bicknell, R. (2005). Tumour vascular targeting. *Nat. Rev. Cancer* **5**, 436-446.

Ohashi, T., Kiehart, D. P. and Erickson, H. P. (2002). Dual labeling of the fibronectin matrix and actin cytoskeleton with green fluorescent protein variants. *J. Cell Sci.* **115**, 1221-1229.

Pankov, R. and Yamada, K. M. (2002). Fibronectin at a glance. *J. Cell Sci.* **115**, 3861-3863.

Pankov, R., Cukierman, E., Katz, B. Z., Matsumoto, K., Lin, D. C., Lin, S., Hahn, C. and Yamada, K. M. (2000). Integrin dynamics and matrix assembly: tensin-dependent translocation of alpha(5)beta(1) integrins promotes early fibronectin fibrillogenesis. *J. Cell Biol.* **148**, 1075-1090.

Paul, R., Zhang, Z. G., Eliceiri, B. P., Jiang, Q., Boccia, A. D., Zhang, R. L., Chopp, M. and Cheresh, D. A. (2001). Src deficiency or blockade of Src activity in mice provides cerebral protection following stroke. *Nat. Med.* **7**, 222-227.

Pereira, M., Rybarczyk, B. J., Odrljin, T. M., Hocking, D. C., Sottile, J. and Simpson-Haidaris, P. J. (2002). The incorporation of fibrinogen into extracellular matrix is dependent on active assembly of a fibronectin matrix. *J. Cell Sci.* **115**, 609-617.

Peters, J. H. and Hynes, R. O. (1996). Fibronectin isoform distribution in the mouse. I. The alternatively spliced EIIIB, EIIIA, and V segments show widespread codistribution in the developing mouse embryo. *Cell Adhes. Commun.* **4**, 103-125.

Peters, J. H., Chen, G. E. and Hynes, R. O. (1996). Fibronectin isoform distribution in the mouse. II. Differential distribution of the alternatively spliced EIIIB, EIIIA, and V segments in the adult mouse. *Cell Adhes. Commun.* **4**, 127-148.

Petrie, R. J., Doyle, A. D. and Yamada, K. M. (2009). Random versus directionally persistent cell migration. *Nat. Rev. Mol. Cell Biol.* **10**, 538-549.

Ramirez, F. and Rifkin, D. B. (2009). Extracellular microfibrils: contextual platforms for TGFbeta and BMP signaling. *Curr. Opin. Cell Biol*. **21**, 616-622.

Roberts, M., Barry, S., Woods, A., van der Sluijs, P. and Norman, J. (2001). PDGF-regulated rab4-dependent recycling of alphavbeta3 integrin from early endosomes is necessary for cell adhesion and spreading. *Curr. Biol.* **11**, 1392-1402.

Scheppke, L., Aguilar, E., Gariano, R. F., Jacobson, R., Hood, J., Doukas, J., Cao, J., Noronha, G., Yee, S., Weis, S. et al. (2008). Retinal vascular permeability suppression by topical application of a novel VEGFR2/Src kinase inhibitor in mice and rabbits. *J. Clin. Invest.* **118**, 2337-2346.

Sechler, J. L., Cumiskey, A. M., Gazzola, D. M. and Schwarzbauer, J. E. (2000). A novel RGD-independent fibronectin assembly pathway initiated by alpha4beta1 integrin binding to the alternatively spliced V region. *J. Cell Sci.* **113**, 1491-1498.

Stanchi, F., Grashoff, C., Nguemeni Yonga, C. F., Grall, D., Fassler, R. and Van Obberghen-Schilling, E. (2009). Molecular dissection of the ILK-PINCH-parvin triad reveals a fundamental role for the ILK kinase domain in the late stages of focal-adhesion maturation. *J. Cell Sci.* **122**, 1800-1811.

Takahashi, S., Leiss, M., Moser, M., Ohashi, T., Kitao, T., Heckmann, D., Pfeifer, A., Kessler, H., Takagi, J., Erickson, H. P. et al. (2007). The RGD motif in fibronectin is essential for development but dispensable for fibril assembly. *J. Cell Biol.* **178**, 167-178.

Tan, M. H., Sun, Z., Opitz, S. L., Schmidt, T. E., Peters, J. H. and George, E. L. (2004). Deletion of the alternatively spliced fibronectin EIIIA domain in mice reduces atherosclerosis. *Blood* **104**, 11-18.

Trinh, L. A. and Stainier, D. Y. (2004). Fibronectin regulates epithelial organization during myocardial migration in zebrafish. *Dev. Cell* **6**, 371-382.

Unemori, E. N., Bouhana, K. S. and Werb, Z. (1990). Vectorial secretion of extracellular matrix proteins, matrix-degrading proteinases, and tissue inhibitor of metalloproteinases by endothelial cells. *J. Biol. Chem.* **265**, 445-451.

Velling, T., Risteli, J., Wennerberg, K., Mosher, D. F. and Johansson, S. (2002). Polymerization of type I and III collagens is dependent on fibronectin and enhanced by integrins alpha 11beta 1 and alpha 2beta 1. *J. Biol. Chem.* **277**, 37377-37381.

Villa, A., Trachsel, E., Kaspar, M., Schliemann, C., Sommavilla, R., Rybak, J. N., Rosli, C., Borsi, L. and Neri, D. (2008). A high-affinity human monoclonal antibody specific to the alternatively spliced EDA domain of fibronectin efficiently targets tumor neo-vasculature in vivo. *Int. J. Cancer* **122**, 2405-2413.

Vouret-Craviari, V., Boulter, E., Grall, D., Matthews, C. and Van Obberghen-Schilling, E. (2004). ILK is required for the assembly of matrix-forming adhesions and capillary morphogenesis in endothelial cells. *J. Cell Sci.* **117**, 4559-4569.

Wayne, J., Sielski, J., Rizvi, A., Georges, K. and Hutter, D. (2006). ERK regulation upon contact inhibition in fibroblasts. *Mol. Cell Biochem.* **286**, 181-189.

Weis, S., Cui, J., Barnes, L. and Cheresh, D. (2004). Endothelial barrier disruption by VEGF-mediated Src activity potentiates tumor cell extravasation and metastasis. *J. Cell Biol.* **167**, 223-239.

White, D. P., Caswell, P. T. and Norman, J. C. (2007). alpha v beta3 and alpha5beta1 integrin recycling pathways dictate downstream Rho kinase signaling to regulate persistent cell migration. *J. Cell Biol.* **177**, 515-525.

White, E. S., Baralle, F. E. and Muro, A. F. (2008). New insights into form and function of fibronectin splice variants. *J. Pathol.* **216**, 1-14.

Whittaker, C. A., Bergeron, K. F., Whittle, J., Brandhorst, B. P., Burke, R. D. and Hynes, R. O. (2006). The echinoderm adhesome. *Dev. Biol.* **300**, 252-266.

Wierzbicka-Patynowski, I. and Schwarzbauer, J. E. (2003). The ins and outs of fibronectin matrix assembly. *J. Cell Sci.* **116**, 3269-3276.

Wijelath, E. S., Rahman, S., Namekata, M., Murray, J., Nishimura, T., Mostafavi-Pour, Z., Patel, Y., Suda, Y., Humphries, M. J. and Sobel, M. (2006). Heparin-II domain of fibronectin is a vascular endothelial growth factor-binding domain: enhancement of VEGF biological activity by a singular growth factor/matrix protein synergism. *Circ. Res.* **99**, 853-860.

Woods, A. J., White, D. P., Caswell, P. T. and Norman, J. C. (2004). PKD1/PKCmu promotes alphavbeta3 integrin recycling and delivery to nascent focal adhesions. *EMBO J.* **23**, 2531-2543.

Wu, C. (2004). The PINCH-ILK-parvin complexes: assembly, functions and regulation. *Biochim. Biophys. Acta* **1692**, 55-62.

Wu, C., Keightley, S. Y., Leung-Hagesteijn, C., Radeva, G., Coppolino, M., Goicoechea, S., McDonald, J. A. and Dedhar, S. (1998). Integrin-linked protein kinase regulates fibronectin matrix assembly, E-cadherin expression, and tumorigenicity. *J. Biol. Chem.* **273**, 528-536.

Yang, J. T., Rayburn, H. and Hynes, R. O. (1993). Embryonic mesodermal defects in alpha 5 integrin-deficient mice. *Development* **119**, 1093-1105.

Zamir, E., Katz, M., Posen, Y., Erez, N., Yamada, K. M., Katz, B. Z., Lin, S., Lin, D. C., Bershadsky, A., Kam, Z. et al. (2000). Dynamics and segregation of cell-matrix adhesions in cultured fibroblasts. *Nat. Cell Biol.* **2**, 191-196.

Zhou, X., Rowe, R. G., Hiraoka, N., George, J. P., Wirtz, D., Mosher, D. F., Virtanen, I., Chernousov, M. A. and Weiss, S. J. (2008). Fibronectin fibrillogenesis regulates three-dimensional neovessel formation. *Genes Dev.* **22**, 1231-1243.

Journal of Cell Science